Zheng et al. Nanoscale Research Letters (2019) 14:281
https://doi.org/10.1186/s11671-019-3112-x

Nanoscale Research Letters

NANO EXPRESS Open Access

Space-Confined Effect One-Pot Synthesis of γ-AlO(OH)/MgAl-LDH Heterostructures with Excellent Adsorption Performance

Guoyuan Zheng[1,2], Caihong Wu[2,3], Jilin Wang[2,3*], Shuyi Mo[1,2], Zhengguang Zou[1,2], Bing Zhou[1,2] and Fei Long[1,2*]

Abstract

Herein, γ-AlO(OH) as an inorganic was successfully inserted into MgAl-LDH layer by a one-pot synthesis, the composite as an adsorbent for removing methyl orange (MO) from wastewater. The structure and adsorption performance of γ-AlO(OH)/MgAl-LDH were characterized. The research shows that the expansion (003) plane and the hydroxyl active site of γ-AlO(OH)/MgAl-LDH can promote adsorption capacity and adsorption kinetics, respectively. Therefore, γ-AlO(OH)/MgAl-LDH exhibits a super adsorption performance, which completely adsorbs MO at the concentration of 1000 mg g^{-1}. In addition, the maximum adsorption capacity of MO was 4681.40 mg g^{-1} according to the Langmuir model. These results indicate that γ-AlO(OH)/MgAl-LDH is a potential adsorbent for the removal of organic dyes in water.

Keywords: γ-AlO(OH)/MgAl-LDH, Space-confined, Langmuir model, Potential adsorbent

Introduction

Organic dyes are widely used in many products such as textiles, leather, paint, and rubber [1–3]. These dyes are easily discharged into water [4], causing serious environmental problems such as harming aquatic organisms, consuming dissolved oxygen, and staining water [3, 5]. In addition, most organic dyes are highly polar, nonvolatile, and difficult to biodegrade. It is observed that dye wastewater is severely detrimental to human health. Therefore, the treatment of dye wastewater is an urgent task. At present, most of the treatments for dye wastewater use physical adsorption, photocatalysis, biological and chemical oxidation, flocculation, and membrane separation [4, 6]. Among them, the physical adsorption method has a special position in the field of wastewater treatment due to its ability to selectively enrich certain compounds. In addition, the adsorption method has the characteristics of a good adsorption effect, simple operation, and wide application range and has been widely used in the field of dye wastewater treatment [7, 8].

Layered double hydroxides (LDHs), a common anionic clay, consist of brucite-like layers [9]. Its general formula can be expressed as $[M^{2+}{}_{1-x}M^{3+}{}_{x}(OH)_2][(A^{n-})_{x/n}]\cdot yH_2O$, where M^{2+}, M^{3+}, and A^{n-} represent the bivalent cations, trivalent cations, and n-valent anions, respectively [10]. LDH has excellent adsorption properties for dyes due to its high anion exchange capacity and large surface area. For example, Lafi et al. prepared MgAl-LDH by a coprecipitation method; the adsorption capacity of the adsorbent on Congo red reached 111.111 mg g^{-1} [11]. Zheng et al. prepared Zn-Mg-Al LDH also via the coprecipitation method, which have an excellent adsorption capacity as high as 883.24 mg g^{-1} for methyl orange at the condition of pH = 3 [12]. Clearly, for LDH adsorbents, most researchers focus on the pursuit of high ion exchange capacity and large specific surface area. Unfortunately, the nanocrystallization of LDHs is not without limits. In recent years, researchers have found that organic or inorganic insert to LDH layers can increase the adsorption capacity of LDH. For example, Mandal et al. inserted sodium alginate between the LDH layers to form a composite adsorbent. The sodium alginate helps in widening the interlayer space of the LDH and increases the adsorption capacity of the adsorbent for the orange II dye [13]. Bruna et al. synthesized organic/LDH (organic anion dodecylsulfate (DDS) insert to MgAl-LDH)

* Correspondence: jilinwang@glut.edu.cn; longf@glut.edu.cn
[2]Guangxi Key Laboratory of Optical and Electronic Materials and Devices, Guilin University of Technology, Guilin 541004, China
[1]Key Laboratory of New Processing Technology for Nonferrous Metals and Materials of Ministry of Education, Guilin University of Technology, Guilin 541004, China
Full list of author information is available at the end of the article

Springer Open

© The Author(s). 2019 **Open Access** This article is distributed under the terms of the Creative Commons Attribution 4.0 International License (http://creativecommons.org/licenses/by/4.0/), which permits unrestricted use, distribution, and reproduction in any medium, provided you give appropriate credit to the original author(s) and the source, provide a link to the Creative Commons license, and indicate if changes were made.

as an adsorbent of polycyclic aromatic hydrocarbons in water and soil-water systems [14]. Therefore, it is a good idea to design the adsorbent by inserting a compound between the LDH layers. Aluminum oxide hydroxide (γ-AlO(OH)) is a good adsorbent for wastewater treatment, due to high specific surface area and large amount of hydroxyl groups on the surface [15, 16]. Hence, γ-AlO(OH) is a potential inorganic intercalation material for MgAl-LDH.

In this paper, γ-AlO(OH) was successfully inserted to MgAl-LDH by a hydrothermal method. This composite exhibits excellent adsorption properties for methyl orange (MO). The structural characteristics of γ-AlO(OH)/MgAl-LDH composites were evaluated using X-ray powder diffraction (XRD), Fourier-transform infrared spectroscopy (FTIR), field-emission scanning electron microscopy (FESEM), transmission electron microscopy (TEM), and high-resolution transmission electron microscopy (HRTEM). The adsorption properties of the composites were evaluated via the adsorption of MO, and in-depth research on the synergistic mechanism of γ-AlO(OH) and MgAl-LDH was conducted.

Methods

Preparation of γ-AlO(OH)/MgAl-LDH

All chemical reagents were of analytical grade and used without further purification. The γ-AlO(OH)/MgAl-LDH composite was prepared using the hydrothermal method. In a typical synthesis, $Mg(NO_3)_2{\cdot}6H_2O$ (4.615 g) and $Al(NO_3)_3{\cdot}9H_2O$ (3.376 g) were dissolved in 50 mL of deionized (DI) water (Mili-Q, 18.2 MΩ) to form solution 1. NaOH (2.516 g) was dissolved in 25 mL of degassed deionized water, such that solution 2 was produced. Solutions 1 and 2 were added dropwise to a reaction vessel containing 25 mL of deionized water, and stirring was performed vigorously at a constant pH value of 10 and a temperature of 60 °C. Then, the resultant slurry was further treated under a hydrothermal condition at 140 °C for 10 h and cooled to room temperature. γ-AlO(OH)/MgAl-LDH was washed several times with deionized water and lyophilized in a vacuum freeze dryer. For comparison, pure MgAl-LDH and γ-AlO(OH) were prepared by the same hydrothermal treatment (140 °C, 10 h).

Characterization

The phase structure was characterized by powder X-ray diffraction (XRD; X'Pert PRO PANalytical) in the 2θ range of 5–80° with Cu Kα radiation at a wavelength of 0.15406 nm. The surface morphology of the sample was imaged by FESEM (S4800) at 5 kV. The microstructure of the samples was analyzed by HRTEM (JEM-2100F) at 200 kV. IR spectra were recorded in the range of 4000–400 cm^{-1} using a FTIR spectrometer (NEXUS 470, Nicolet instruments) with an optical resolution of 4 cm^{-1} and an aperture size of 100 im. Nitrogen adsorption-desorption experiments for surface and porosity quantification were performed at − 196 °C with a NOVA-1200e instrument. Prior to analysis, samples were pretreated at 80 °C for 12 h under vacuum. X-ray photoelectron spectroscopy (XPS; ESCALAB 250Xi) measurements were performed using Al Kα radiation. The energy of survey spectrum scanning was 100 eV by the step size of 1 eV. The energy of high-resolution scanning was 20 eV by the step size of 0.1 eV. The vacuum of the test is 10^{-10} mbar. The UV–Vis absorption spectra of the different samples were obtained using a UV-3600 spectrophotometer equipped with an integrating sphere. The photoluminescence spectra of the materials were obtained by a fluorescence spectrophotometer (VARIAN).

Adsorption Experiments

The adsorption performance of the samples was tested for the adsorption of methyl orange (MO) in aqueous solution. A 50-mg sample was placed in 50 mL of 1000 mg L^{-1} MO solution under magnetic stirring. The pH value of the solution was adjusted using 0.1 M HNO_3 acid or 1 M NaOH solution. After an appropriate time, the water sample (3 mL) was taken from the suspension. The supernatant was obtained by centrifugation, and the concentration of the solution was measured using a UV–Vis spectrophotometer (UV-3600). The equilibrium amount of adsorption (q_e (mg g^{-1})) and the instantaneous amount of adsorption (q_t (mg g^{-1})) were calculated by the following equations:

$$q_t = \frac{(C_0 - C_t)V}{m}$$

$$q_e = \frac{(C_0 - C_e)V}{m}$$

where C_0 (mg L^{-1}) is the initial MO concentration; C_e (mg L^{-1}) and C_t(mg L^{-1}) are the MO concentration at equilibrium and at time t (min), respectively; V (L) is the volume of the solution; and m (g) is the mass of the adsorbent.

Desorption Experiments

The desorption experiment of MO was performed using DI water as a disturbing agent. A 50-mg portion of the used samples was washed gently with water to remove any undisturbed MO. In addition, loaded MO samples were stirred vigorously with ethanol solution and centrifuged. After centrifugation, the obtained samples were lyophilized. Then, the resulting powder samples were subjected to successive adsorption-desorption cycles.

Results and Discussion

Characterization of As-Synthesized Samples

The XRD patterns of the as-synthesized samples are shown in Fig. 1a. For γ-AlO(OH)/MgAl-LDH, it is observed that the major diffraction peaks are at 10.09°, 19.95°, 34.40°, 60.56°, and 61.48°, which corresponded to the (003), (006), (012), (110), and (113) planes of MgAl-LDH (JPCDS No. 89-0460), respectively. In addition, the peaks at 14.1°, 27.9°, 38.1°, and 48.9° can be attributed to the (020), (120), (031), and (051) diffraction planes of γ-AlO(OH) (JPCDS No. 21-1307), respectively. This result indicates that the γ-AlO(OH)/MgAl-LDH composite has MgAl-LDH and γ-AlO(OH) phases. Moreover, for comparison, the (003) plane of MgAl-LDH is located at 2θ = 11.63°, indicating that when γ-AlO(OH) was inserted into MgAl-LDH, the spacing of the (003) plane increased from 7.6 Å (2θ = 11.63°) to 8.77 Å (2θ = 10.09°). The unit cell parameters are shown in Table 1. It is observed that the "a" axes of MgAl-LDH and γ-AlO(OH)/MgAl-LDH have not changed.

The FTIR spectra of the as-synthesized samples are shown in Fig. 1b. In the FTIR spectrum of MgAl-LDH, the band at 3449 cm^{-1} can be attributed to the O–H stretching vibration [17]. The bands from 400 to 900 cm^{-1} are due to M–O, O–M–O, and M–O–M (M = Mg^{2+} and Al^{3+}) stretching vibrations [18], and the band at 781 cm^{-1} is due to an Al–OH vibration [19]. For γ-AlO(OH), the bands at 3111 and 3325 cm^{-1} belong to the υas(Al)O–H and υs(Al)O–H stretching vibrations, respectively [20]. The vibrations of hydrogen bonds were observed at 1142 and 1066 cm^{-1} [21]. In addition, the peaks at 481, 636, and 749 cm^{-1} can be assigned to Al–O bonds [22]. For γ-AlO(OH)/MgAl-LDH, most of the bands can be easily assigned based on the comparison with γ-AlO(OH) and MgAl-LDH. The strong band at 3474 cm^{-1} can be attributed to the stretching vibration of the –OH groups in γ-AlO(OH) and MgAl-LDH. The bands at 826, 669, and 445 cm^{-1} correspond to metal-oxygen, metal-oxygen-metal, and oxygen-metal-oxygen stretching vibrations in MgAl-LDH, respectively [18]. Compared with MgAl-LDH, the band of Al–OH is shifted from 781 to 826 cm^{-1}. In addition, the band at 1064 cm^{-1} can be assigned to the vibration of the hydrogen bond in γ-AlO(OH). The bands at 1618, 1633, and 1619 cm^{-1} in MgAl-LDH, γ-AlO(OH), and γ-AlO(OH)/MgAl-LDH, respectively, can be assigned to the bending vibration of the water molecules. In addition, the bands at 1360, 1385, and 1380 cm^{-1} in MgAl-LDH, γ-AlO(OH), and γ-AlO(OH)/MgAl-LDH, respectively, are related to CO_3^{2-} [23]. The band of CO_3^{2-} in γ-AlO(OH) indicates that some carbonate-based residuals remain trapped inside the highly porous cellular monolith even after repeated washing [24].

The morphology and microstructure of the samples were investigated by field-emission scanning electron microscopy (FESEM) and transmission electron microscopy (TEM). As shown in Fig. 2a, it is observed that the MgAl-LDH sample consists of nanosheets. The average thickness of the nanosheets is estimated to be between 140 and 150 nm. The FESEM image in Fig. 2b shows that γ-AlO(OH) consists of nanoneedles. The γ-AlO(OH)/MgAl-LDH sample shown in Fig. 2c has a morphology consisting of flaky agglomerates rather than the morphology of γ-AlO(OH). In the case of Fig. 2d, e, the TEM images of MgAl-LDH and γ-AlO(OH), respectively, also show strong evidence of the nanosheet-like morphology of MgAl-LDH and the nanoneedle-like morphology of γ-AlO(OH). Interestingly, it is clearly observed that the γ-AlO(OH)/MgAl-LDH sample consists of nanosheets and nanoneedles (Fig. 2f). In addition, in the HRTEM image of γ-AlO(OH)/MgAl-LDH (Fig. 2g), the lattice spacing 0.235 nm and 0.152 nm corresponded to the (031) plane of γ-AlO(OH) and (110) plane of MgAl-LDH. In addition, EDX mapping of Fig. 2h, i demonstrated the uniform distribution of C, O, Mg, and Al elements in composites, indicating that γ-AlO(OH)/MgAl-LDH composite was mixed homogeneously.

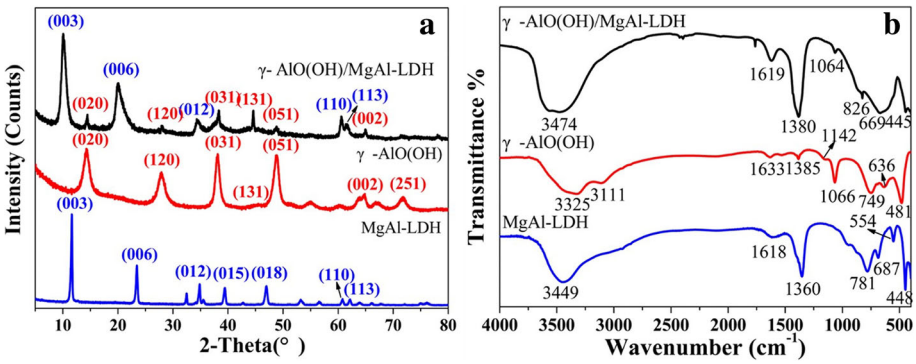

Fig. 1 XRD patterns of as-synthesized samples (**a**). The FTIR spectra of as-synthesized samples at 400–4000 cm^{-1} (**b**)

Table 1 Unit cell parameters, crystallite size, surface area, pore volume, and average pore diameter of the samples

Sample	Unit cell parameters (Å)		Crystallite size[a] (nm)		Surface area[b] (m^2 g^{-1})	Pore volume[b] (cm^3 g^{-1})	Average pore size[b] (nm)
	a	c	D_{003}	D_{110}			
MgAl-LDH	3.05	22.8	31.0	26.6	14.1	0.017	5.2
γ-AlO(OH)	n.a.	n.a.	n.a.	n.a.	95.9	0.122	4.9
γ-AlO(OH)/MgAl-LDH	3.05	26.3	10.3	26.6	34.1	0.052	6.2

$a = 2d_{110}$, $c = 3d_{003}$
[a]Obtained from the Debye-Scherrer formula
[b]Calculated from the BET analysis

The XRD, FTIR, FESEM, and HRTEM analyses show that the nanoneedle γ-AlO(OH) was successfully prepared in the MgAl-LDH layers by the hydrothermal method, which takes advantage of the "space-confined" effect of MgAl-LDH.

Effect of the Initial Solution pH

The pH of the solution plays an important role in the adsorption process due to the surface charge of the adsorbent [25]. Figure 3 shows the adsorption performance of the γ-AlO(OH)/MgAl-LDH sample on MO under different pH values, with the initial MO concentration at 1000 mg L^{-1}. It is observed that the highest adsorption occurs when the initial pH = 3, and the adsorption capacity decreases with increasing pH, indicating that the as-synthesized sample is more effective at adsorbing MO in acidic solution. Furthermore, the structures of the layered

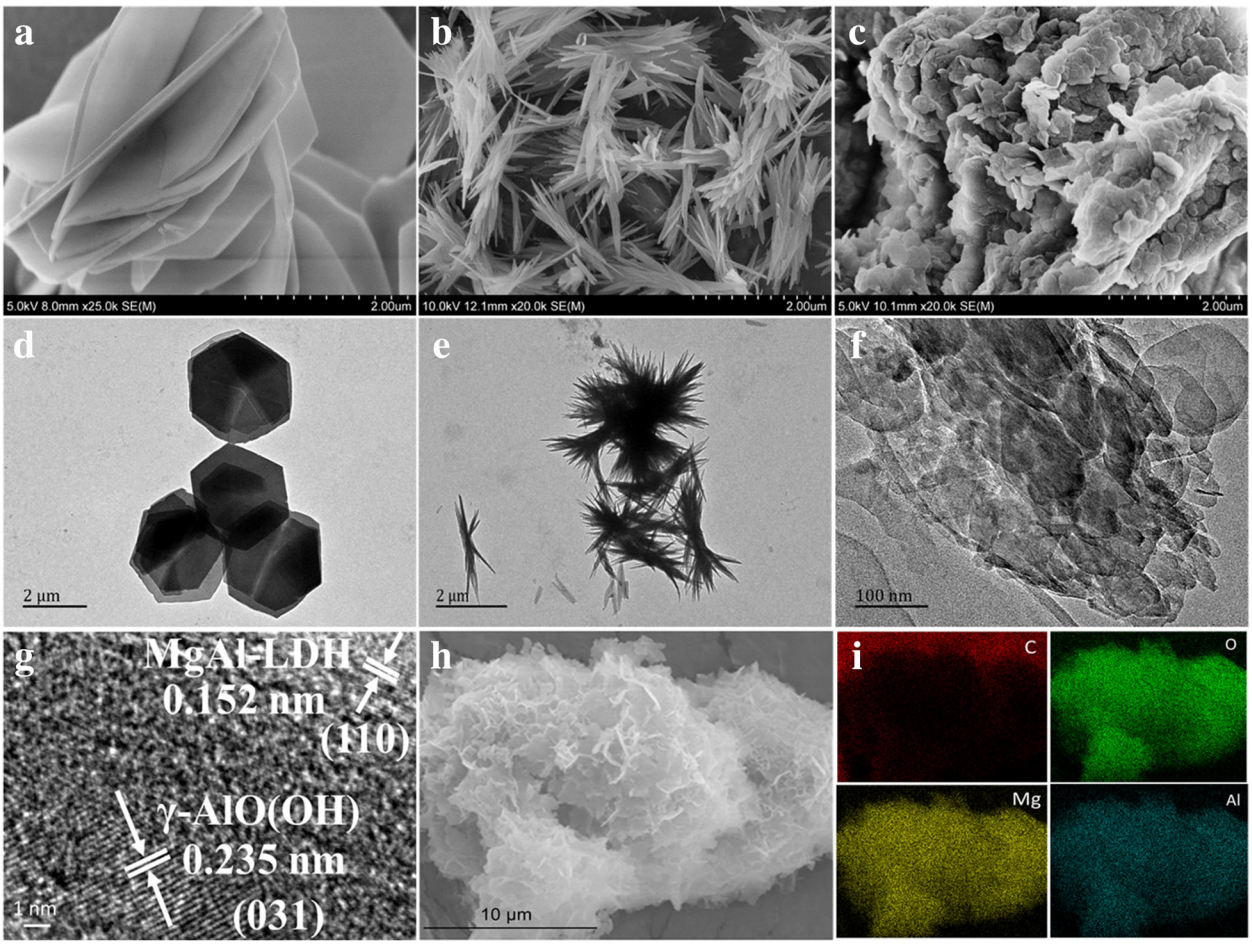

Fig. 2 FESEM images of MgAl-LDH (**a**), γ-AlO(OH) (**b**), and γ-AlO(OH)/MgAl-LDH (**c**). TEM images of MgAl-LDH (**d**), γ-AlO(OH) (**e**), and γ-AlO(OH)/MgAl-LDH (**f**). HRTEM image (**g**) and EDX mapping (**h**, **i**) of γ-AlO(OH)/MgAl-LDH

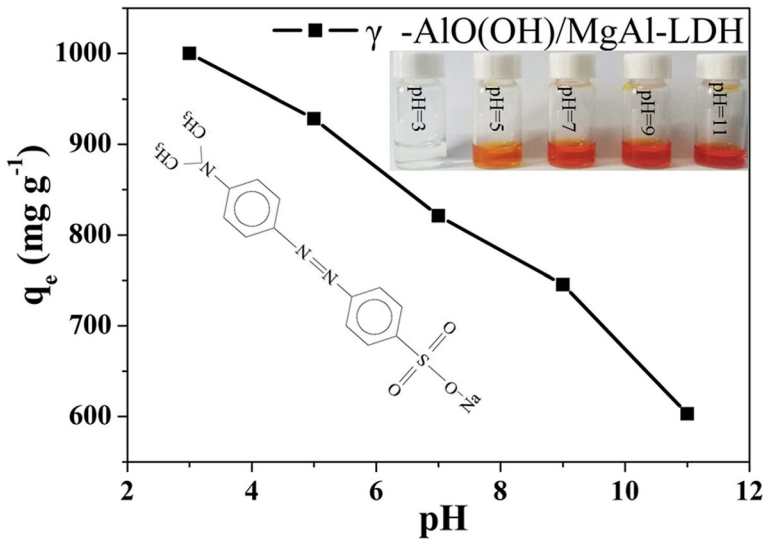

Fig. 3 Effect of initial solution pH values on the adsorption of MO of γ-AlO(OH)/MgAl-LDH (initial MO concentration: 1000 mg L^{-1}, adsorbent dosage: 1 g L^{-1}, contact time: 210 min), inset: the optical photographs of MO solution after adsorbed at different pH

materials with hydroxide sheets vanish when the pH is below 3 [26]. Therefore, the initial solution pH used in this study is suggested to be 3. Photographs of the γ-AlO(OH)/MgAl-LDH sample adsorbing MO at different pH values are also shown in Fig. 3 (inset). It is observed that at pH = 3, after MO was adsorbed for 210 min, the color of the solution was clear, indicating that MO was completely adsorbed. As the pH increased, the color of the solution became darker.

Effect of the Contact Time and the Kinetics of Adsorption

The effect of the contact time on the MO adsorption by the samples is shown in Fig. 4. For all adsorbents, the initial rates of adsorption are very fast. Compared with pure γ-AlO(OH) and MgAl-LDH, γ-AlO(OH)/

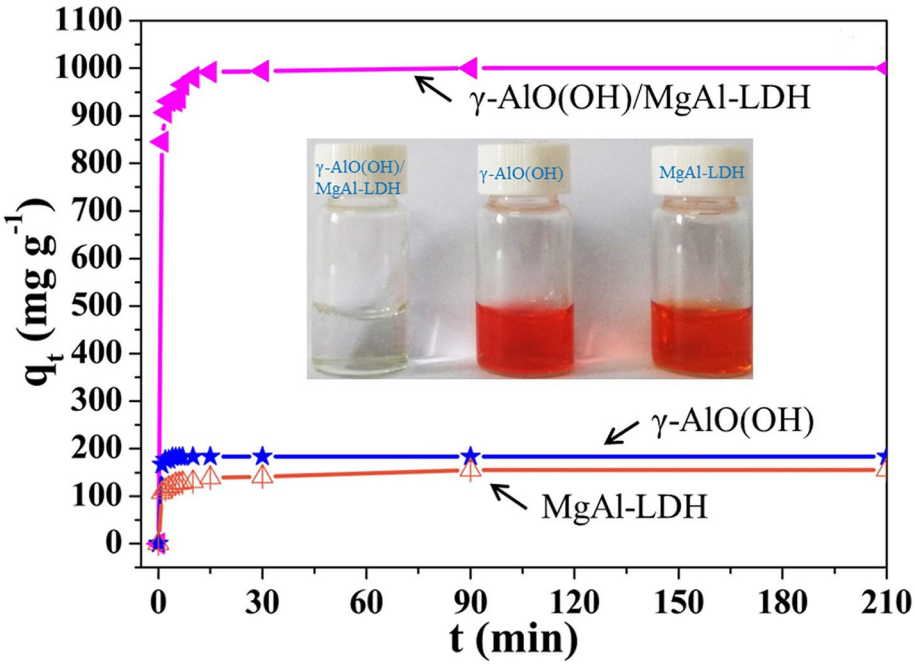

Fig. 4 Effect of contact time on MO adsorption, inset: the equilibrium optical photographs of MO solution after adsorbed

MgAl-LDH shows an enhanced adsorption performance in terms of the adsorption speed and capacity. When the initial concentration of MO was 1000 mg L^{-1} for γ-AlO(OH)/MgAl-LDH and 200 mg L^{-1} for γ-AlO(OH) and MgAl-LDH, the maximum experimental equilibrium adsorption capacity of 1000 mg g^{-1} was obtained using γ-AlO(OH)/MgAl-LDH, which was higher than that of γ-AlO(OH) (183.3 mg g^{-1}) and MgAl-LDH (155.5 mg g^{-1}). As shown in the Fig. 4 (inset), it is observed that the γ-AlO(OH)/MgAl-LDH solution is completely colorless after equilibration. However, the colors of the pure γ-AlO(OH) and MgAl-LDH solutions remain very deep.

To understand the adsorption mechanisms of the samples, kinetic models of pseudo-first-order and pseudo-second-order were used to fit the experimental data. The pseudo-first-order and pseudo-second-order rate laws are calculated from Eqs. (3) and (4) [27], respectively:

$$\ln(q_e - q_t) = \ln q_e - k_1 t \quad (3)$$

$$\frac{t}{q_t} = \frac{1}{k_2 q_e^2} + \frac{t}{q_e} \quad (4)$$

where q_t (mg g^{-1}) and q_e (mg g^{-1}) are the amount of adsorbed MO at time t (min) and at equilibrium, respectively, and k_1 (min^{-1}) and k_2 (g mg^{-1} min^{-1}) are the adsorption rate constants of the pseudo-first-order and pseudo-second-order kinetic models [28], respectively.

Table 2 shows the two adsorption kinetic models and correlation coefficients. From the correlation coefficient R^2 in Table 2, it is observed that the adsorption of samples was fitted better by the pseudo-second-order model than by the pseudo-first-order model. In addition, the theoretical calculated values ($q_{e,cal}$) from the pseudo-second-order model are closer to the experimental values ($q_{e,exp}$) than those of the pseudo-first-order model. Therefore, based on the assumption of pseudo-second-order kinetics, the adsorption rates of MgAl-LDH, γ-AlO(OH), and γ-AlO(OH)/MgAl-LDH are controlled by chemical interactions [29].

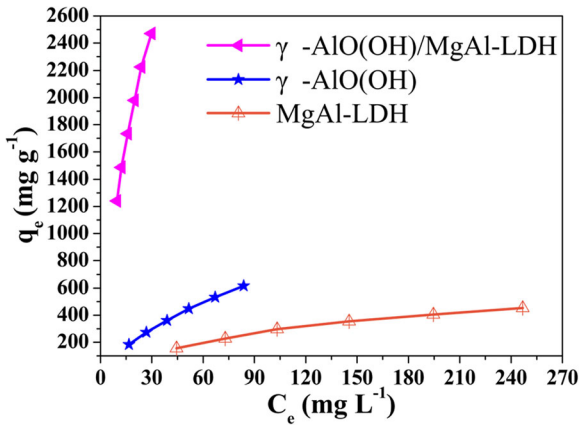

Fig. 5 The equilibrium adsorption isotherms of the samples

Adsorption Isotherms

Figure 5 shows the adsorption isotherms of the as-synthesized samples. Among the three samples, the q_e value of γ-AlO(OH)/MgAl-LDH exhibited the fastest increase with C_e. In addition, the adsorption experiment data were analyzed via the Langmuir and Freundlich models to evaluate the relationship between MO and adsorbents at equilibrium [30]. The equations are as follows:

$$\text{Langmuir}: \frac{C_e}{q_e} = \frac{1}{q_m K_L} + \frac{C_e}{q_m}$$

$$\text{Freundlich}: \ln q_e = \ln K_F + \frac{1}{n} \ln C_e$$

where C_e (mg L^{-1}) is the equilibrium concentration of the MO, q_e (mg g^{-1}) is the amount of MO adsorbed per unit mass of the adsorbents, and q_m (mg g^{-1}) is the monolayer adsorption capacity. K_L (L mg^{-1}) is the

Table 2 Kinetic parameters for the adsorption of MO onto MgAl-LDH, γ-AlO(OH), and γ-AlO(OH)/MgAl-LDH

Kinetic models	Parameters	MgAl-LDH	γ-AlO(OH)	γ-AlO(OH)/MgAl-LDH
Pseudo-first-order	q_e (mg g^{-1}) experiment	155.5	183.3	1000
	q_e (mg g^{-1}) model	48.6	40.9	146.7
	K_1 (min^{-1})	0.05537	0.64079	0.13575
	R^2	0.50311	0.86471	0.65129
Pseudo-second-order	q_e (mg g^{-1}) model	156.5	183.5	1001.3
	K_2 (g mg^{-1} min^{-1})	0.00523	0.11053	0.00450
	R^2	0.9998	1	1

Table 3 Parameters of two types of isothermal models of MO adsorbed on MgAl-LDH, γ-AlO(OH), and γ-AlO(OH)/MgAl-LDH

Isothermal models	Parameters	MgAl-LDH	γ-AlO(OH)	γ-AlO(OH)/MgAl-LDH
Langmuir	K_L (L mg^{-1})	0.00582	0.00830	0.03741
	q_m (mg g^{-1})	769.2	1492.5	4681.4
	R^2	0.99648	0.9977	0.99639
Freundlich	K_F [(mg g^{-1})(L mg^{-1})$^{1/n}$]	15.6	22.6	319.0
	n^{-1}	0.62077	0.75255	0.60843
	R^2	0.98187	0.99748	0.99563

Langmuir constant related to the rate of adsorption. K_F [(mg g^{-1}) (L mg^{-1})$^{1/n}$] and n^{-1} (dimensionless) are Freundlich constants related to the adsorption capacity and adsorption strength, respectively.

The corresponding parameters of the simulated adsorption isotherms of the samples are listed in Table 3. It is observed that the maximum adsorption capacity of MO on γ-AlO(OH)/MgAl-LDH was significantly higher than that on γ-AlO(OH) and MgAl-LDH. Moreover, compared to the Freundlich model, the Langmuir model fits better with the experimental data and has a higher R^2. The q_m of γ-AlO(OH)/MgAl-LDH (4681.40 mg g^{-1}) from the Langmuir equation is much higher than those of γ-AlO(OH) (1492.5 mg g^{-1}) and MgAl-LDH (769.2 mg g^{-1}). In addition, the larger K_F from the Freundlich equation also indicates that γ-AlO(OH)/MgAl-LDH has an enhanced affinity for MO. Surprisingly, the adsorption capacity of γ-AlO(OH)/MgAl-LDH was much higher than most of those reported (as shown in Table 4).

The Adsorption Mechanism of γ-AlO(OH)/MgAl-LDH for MO

Figure 6a, b shows the N_2 adsorption-desorption isotherms and BJH pore size distribution of samples. According to the IUPAC classification, the isotherms can be categorized as IV curves with H3 hysteresis loops at high relative pressure. It is proved that adsorbents have the properties of mesoporous material.

Table 4 Comparison of the maximum adsorption capacity for MO with other adsorbents

Adsorbents	pH	q_m (mg g^{-1})	References
ZnAl-LDO	6.0	181.90	[31]
$CoFe_2O_4$/MgAl-LDO	6.0	1219.51	[2]
Graphene oxide	3.0	16.83	[32]
Chitosan/Al_2O_3/magnetite composite	6.0	416.00	[33]
rGO/Ni/MMO	n.a.	210.80	[7]
Ni-Cr LDH	n.a.	312.50	[34]
Mg_2/Fe-CLDH	n.a.	194.90	[35]
G-LDH	4.5	443.50	[8]
G-LDO	4.5	1062.30	[8]
γ-AlO(OH)/MgAl-LDH	3.0	4681.40	This work

The pore size distribution calculated by the BJH method is shown in Fig. 6b. Compared with MgAl-LDH, γ-AlO(OH) and γ-AlO(OH)/MgAl-LDH have wider pore size distribution curves. As shown in Table 1, BET analysis results of MgAl-LDH, γ-AlO(OH), and γ-AlO(OH)/MgAl-LDH were 14.1 m^2 g^{-1}, 95.9 m^2 g^{-1}, and 34.1 m^2 g^{-1}, respectively. The results demonstrated that the excellent adsorption performance of γ-AlO(OH)/MgAl-LDH does not depend on the large specific surface area. The optical photographs of the samples before and after adsorbing for MO are shown in Fig. 6c (before centrifugation). According to the optical photographs before adsorption, the original volume of the sample was γ-AlO(OH)/MgAl-LDH < γ-AlO(OH) < MgAl-LDH. However, after the adsorption of MO (1000 mg L^{-1}), it was obvious that the volume of powders has changed. The volume expansion rate of the samples was as follows: γ-AlO(OH)/MgAl-LDH > γ-AlO(OH) > MgAl-LDH. Therefore, it could be inferred that the volume expansion rate of the adsorbent has a great influence on the adsorption performance of MO.

Figure 7a shows the XRD patterns of γ-AlO(OH)/MgAl-LDH before and after MO adsorption. Compared with γ-AlO(OH)/MgAl-LDH, many new peaks appeared in the spectra of γ-AlO(OH)/MgAl-LDH after MO adsorption. In addition, except for the (003) and (006) planes of MgAl-LDH, the other planes were not shifted to a low angle. The new peaks indicate that the MO anions enter the interlayer of γ-AlO(OH)/MgAl-LDH via anion exchange and lead to a shift of the (003) plane to the minor angle plane [8]. More importantly, the (003) plane of γ-AlO(OH)/MgAl-LDH increased by 3.22 Å from 8.77 to 11.99 Å after MO adsorption. Interestingly, as shown in Fig. 7b, the degree corresponding to the (003) plane of MgAl-LDH did not change after adsorbing MO, indicating that MO cannot be adsorbed in MgAl-LDH layers. It is observed that γ-AlO(OH) plays an important role in the LDH layer, and the adsorption effect on MO is shown in Scheme 1. On the one hand, by the "space confined" effect, nanoneedle γ-AlO(OH) can be grown between the MgAl-LDH layers to expand the (003) plane spacing, which helps MO to enter the MgAl-LDH intermediate layer by electrostatic attraction.

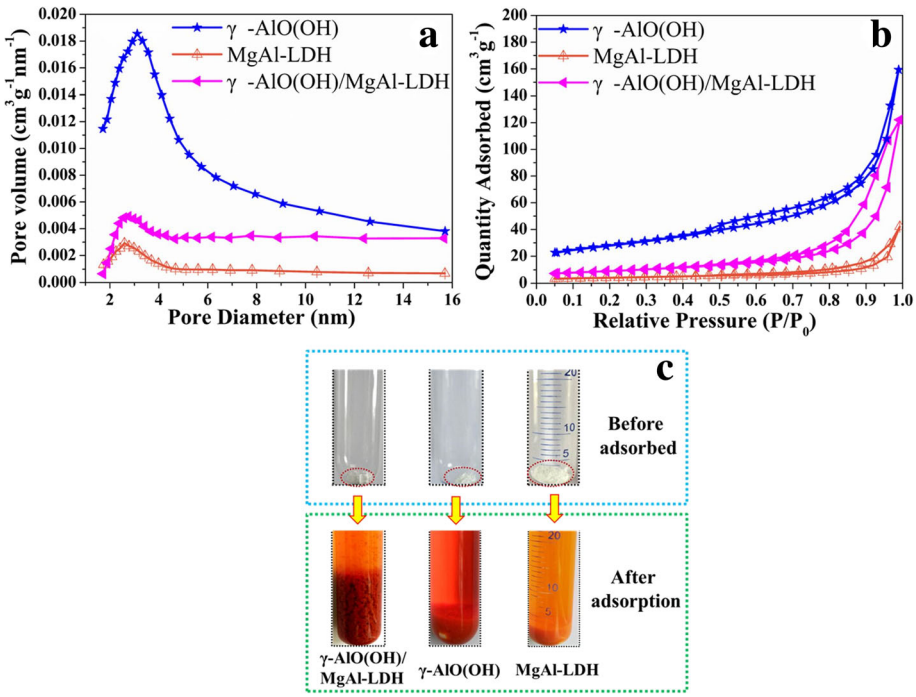

Fig. 6 N_2 adsorption-desorption isotherm curves (**a**) and pore size distribution curves (**b**) of samples. The optical photographs of samples before and after adsorbed (**c**)

On the other hand, MgAl-LDH has more space for storing MO, due to the expansion between the LDH layers.

From the above discussion, it is known that γ-AlO(OH)/MgAl-LDH has a higher adsorption kinetics and adsorption performance than γ-AlO(OH) and MgAl-LDH. To better study the mechanism of performance improvement, the samples were subjected to a zeta potential test. As shown in Fig. 8a, the suspension of the samples at pH = 3 showed a positively charged surface and the ζ-potential value of γ-AlO(OH)/MgAl-LDH (43.03 mV) was much greater than that of MgAl-LDH (13.88 mV) and γ-AlO(OH) (4.32 mV). This result indicates that the synergistic effect can be produced due to γ-AlO(OH) entering the MgAl-LDH layer, which improves the zeta potential of the γ-AlO(OH)/MgAl-LDH sample. As shown in Scheme 1, the MO molecule can be formed to $C_{14}H_{14}N_3SO_3^-$ and Na^+ in water. Because $C_{14}H_{14}N_3SO_3^-$ anion is negatively charged, it is easily to be adsorbed by γ-AlO(OH)/MgAl-LDH. It could be inferred that LDH presents a good adsorption capacity for anionic dyes.

The FTIR spectra of γ-AlO(OH)/MgAl-LDH after adsorbing MO is shown in Fig. 8b. Compared with the original γ-AlO(OH)/MgAl-LDH, the FTIR spectra of γ-AlO(OH)/MgAl-LDH showed obvious changes after absorbing MO. The bands at 1608 and 1520 cm^{-1} were due to the N=N stretching vibration and the N–H bending vibration. In addition, the bands at 1183 and 1033

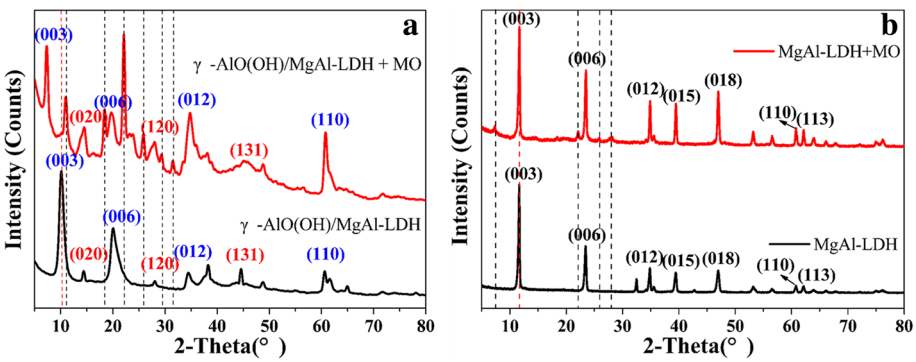

Fig. 7 The XRD patterns of γ-AlO(OH)/MgAl-LDH (**a**) and MgAl-LDH (**b**) before and after adsorbed MO, respectively

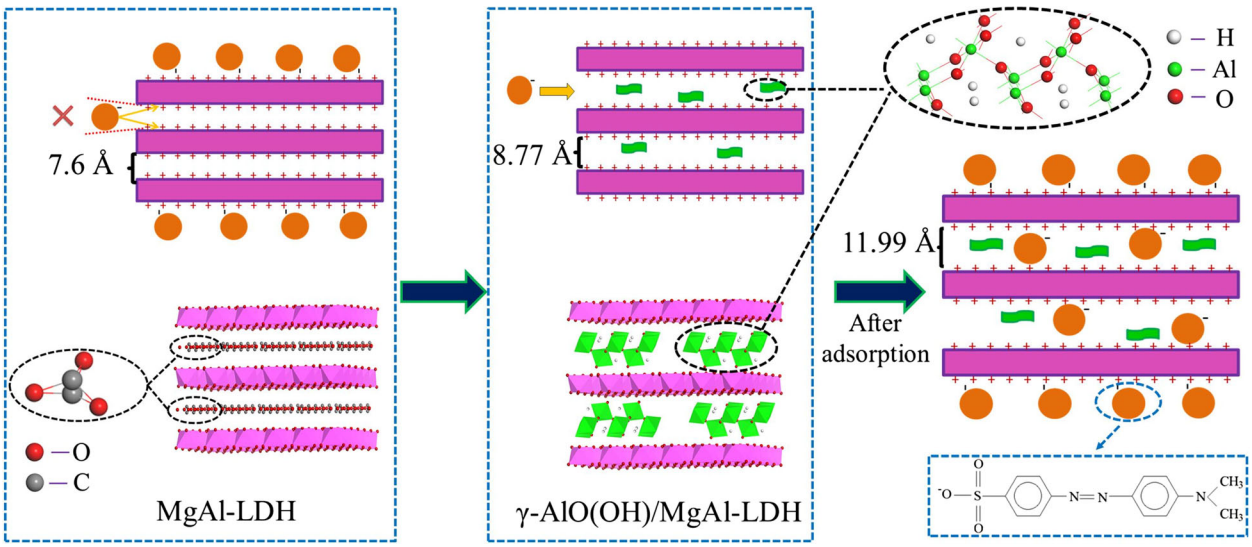

Scheme 1 The mechanism of γ-AlO(OH)/MgAl-LDH for enhancing adsorption of MO

cm^{-1} were due to the asymmetric and symmetric stretching vibrations of the sulfonic acid group ($-SO_3^-$), respectively. The band at 1122 cm^{-1} was due to the symmetrical stretching vibration of O=S=O [36]. The band at 1008 cm^{-1} was related to the C–H aromatic in-plane bending vibration [1]. Obviously, the O–H peak of γ-AlO(OH)/MgAl-LDH was shifted from 3474 to 3843 cm^{-1} when MO was absorbed, indicating that hydrogen bonding participates in the adsorption process.

In addition, XPS was used to characterize the adsorbent before and after adsorbing MO. As shown in Fig. 9, the S element appeared in the spectrum of γ-AlO(OH)/MgAl-LDH after adsorbing MO. The high-resolution spectrum of S 2p located at 167 eV, shown in Fig. 9b, indicates the presence of MO in the adsorbent. Figure 9c, d shows the O 1s spectrum of γ-AlO(OH)/MgAl-LDH before and after MO adsorption, respectively. Three peaks located at 530.5, 531, and 531.8 eV are shown in Fig. 9c, d, and can be assigned to the O in the forms of metal oxide (M–O), the carbonate (CO_3^{2-}), and metal-hydroxyl (M–OH) of the MgAl-LDH interlayer [1]. Notably, there are significant changes in the intensity and composition of O 1s of the adsorbent after MO adsorption. The newly appearing peak located at 531.6 eV in Fig. 9d could be assigned to the O in the sulfate group (S–O). In addition, as shown in Table 5, the CO_3^{2-} decreased from 27.2 to 18.1%, due to ion exchange. The relative proportion of M–O after adsorbing MO is increased from 9 to 26.4%, and the relative proportion of M–OH decreased from 63.8 to 25.7%. The results show that the hydroxyl active site of γ-AlO(OH)/MgAl-LDH plays an important role in the adsorption of methyl

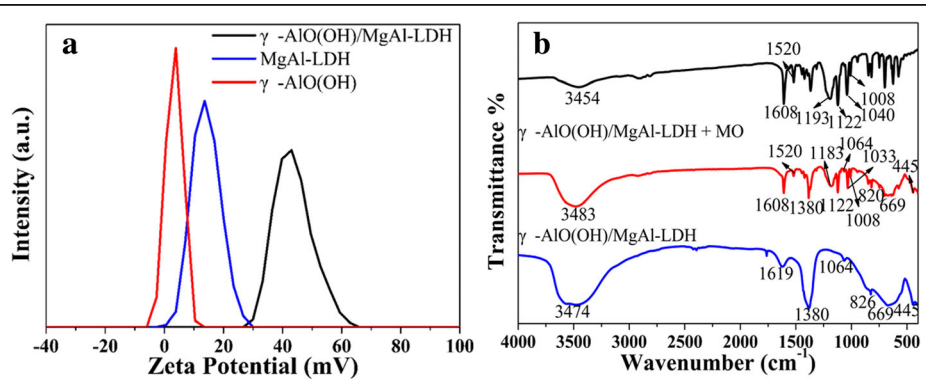

Fig. 8 ζ-potentials of samples (0.2 mg mL^{-1}) in aqueous solution at pH = 3 (**a**). FTIR spectra of MO, γ-AlO(OH)/MgAl-LDH before and after adsorbed MO (**b**)

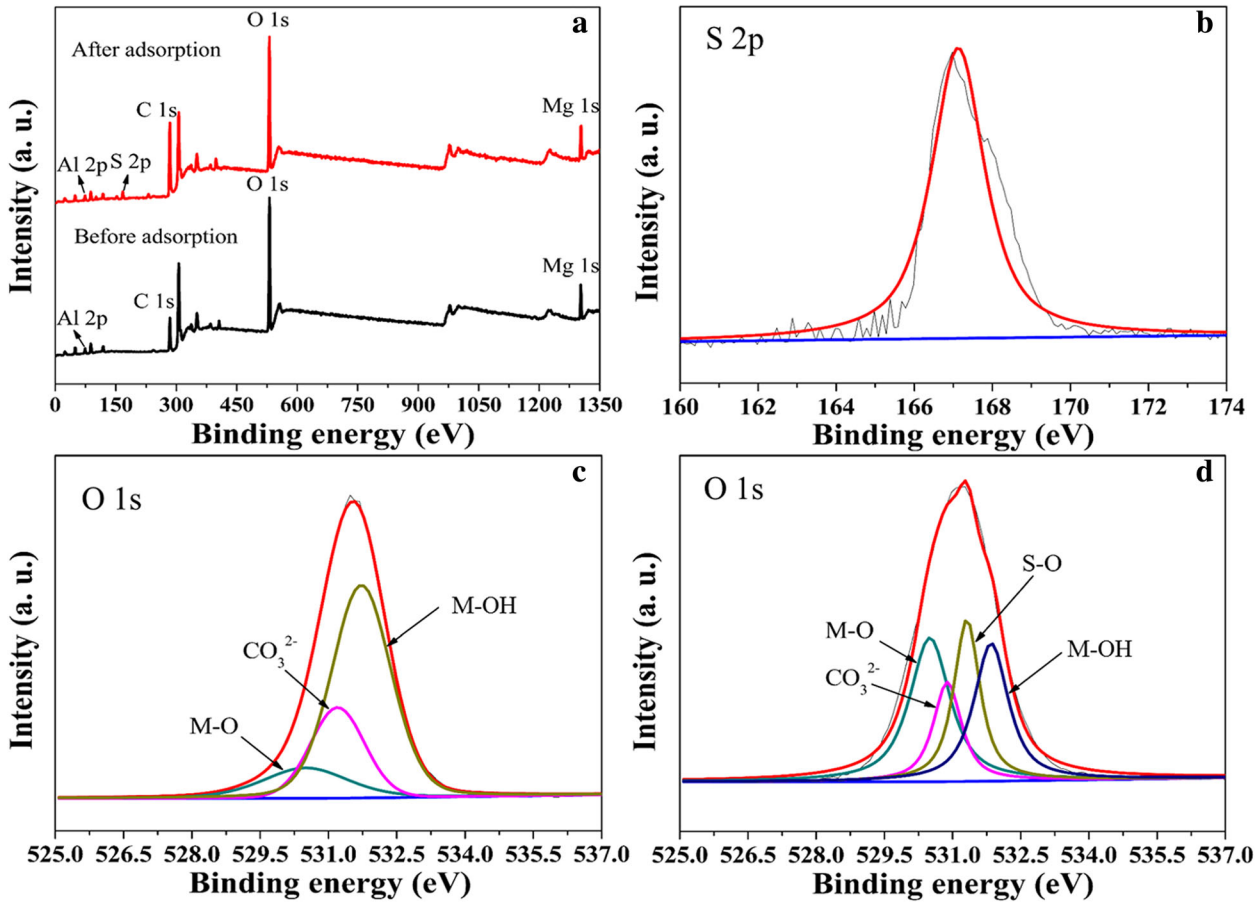

Fig. 9 Wide XPS spectra of γ-AlO(OH)/MgAl-LDH before and after MO adsorption (**a**), S 2p narrow XPS of γ-AlO(OH)/MgAl-LDH after adsorbed MO (**b**), O 1s spectrum of γ-AlO(OH)/MgAl-LDH (**c**), O 1s spectrum of γ-AlO(OH)/MgAl-LDH after adsorbed MO (**d**)

orange, indicating that adsorption of MO is controlled by chemical interactions; this is consistent with the pseudo-second-order kinetic model.

Adsorbent Recycling

The regeneration performance of the γ-AlO(OH)/MgAl-LDH adsorbent was studied via adsorption-desorption cycles. As shown in Fig. 10, the adsorption capacity of γ-AlO(OH)/MgAl-LDH remained at 762 mg g^{-1} after 4 cycles, and the removal efficiency remained above 76%. The decrease in capacity is due to the incomplete desorption of MO and the loss of the adsorbent during the adsorption and washing of the dye molecules. These results indicate that γ-AlO(OH)/MgAl-LDH can be considered an efficient and recyclable adsorbent for the removal of MO from water.

Conclusion

The composite of γ-AlO(OH)/MgAl-LDH was synthesized by one-pot method. As an adsorbent, the

Table 5 Distribution of components from XPS spectra of O 1s peak of adsorbent before and after MO adsorption

Samples	Peak	Binding energy (eV)	Percent (%)
γ-AlO(OH)/MgAl-LDH	CO_3^{2-}	531	27.2
	M–O	530.5	9
	M–OH	531.8	63.8
γ-AlO(OH)/MgAl-LDH after MO adsorption	CO_3^{2-}	531	18.1
	M–O	530.5	26.4
	M–OH	531.8	25.7
	S–O	531.6	29.8

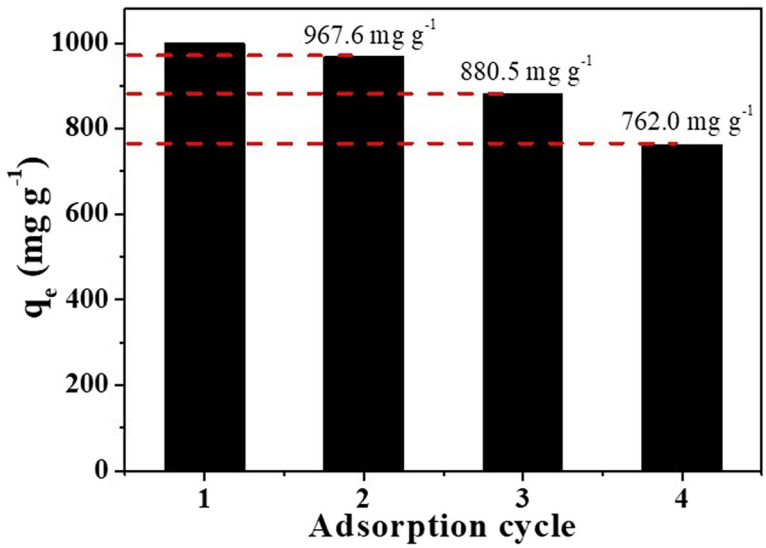

Fig. 10 Adsorption cycle performance of γ-AlO(OH)/MgAl-LDH. Initial MO concentration: 1000 mg L^{-1}

composite exhibits an excellent adsorption performance for MO. On the one hand, based on the "space-confined" effect, γ-AlO(OH) nanoneedle was prepared between the MgAl-LDH layers. The expansion between the LDH layers leads to more space for storing MO. On the other hand, the hydroxyl active site results in a chemical interaction between γ-AlO(OH)/MgAl-LDH and MO, which promotes the adsorption kinetics. Therefore, the γ-AlO(OH)/MgAl-LDH exhibits an excellent adsorption performance for MO, which can be completely adsorbed in 210 min at the initial concentration of 1000 mg L^{-1}. After 4 cycles, the regenerated adsorbent can maintain an initial adsorption capacity of more than 76%. In addition, the maximum adsorption capacity of γ-AlO(OH)/MgAl-LDH reaches 4681.40 mg g^{-1} according to the Langmuir adsorption model. Based on the positive zeta potential of γ-AlO(OH)/MgAl-LDH, the composite has stronger adsorption kinetics and adsorption properties for anionic dyes such as MO, Congo Red, and Acid Orange 7. These adsorbed dyes can be desorbed and reutilization, or incinerated directly. In addition, the composite is also a potential photocatalyst carrier. When the photocatalyst is loaded on γ-AlO(OH)/MgAl-LDH, the dyes will be rapidly absorbed around the catalyst, which improves the photocatalytic reaction kinetics. Therefore, γ-AlO(OH)/MgAl-LDH has great potential in water pollution treatment.

Abbreviations

DDS: Organic anion dodecylsulfate; DI: Deionized; FESEM: Field-emission scanning electron microscopy; FTIR: Fourier-transform infrared spectroscopy; HRTEM: High-resolution transmission electron microscopy; LDHs: Layered double hydroxides; MO: Methyl orange; TEM: Transmission electron microscopy; XPS: X-ray photoelectron spectroscopy; XRD: X-ray powder diffraction; γ-AlO(OH): Aluminum oxide hydroxide

Acknowledgements

We acknowledge the financial support from the National Natural Science Foundation of China (No. 51672052), Guangxi Distinguished Experts Special Fund and Guangxi Graduate Education Innovation Program (No. BS201603).

Author's Contributions

GZ contributed to the experimental studies, analyzed the data, and contributed to manuscript writing. CW, JW, and SM contributed to the sample testing and data collection. ZZ and BZ contributed to the scientific discussion. FL conceived and designed the experiments. All authors read and approved the final manuscript.

Author's Information

Not applicable.

Funding

National Natural Science Foundation of China (No.51672052).

Availability of Data and Materials

The datasets generated during and/or analyzed during the current study are available from the corresponding author on reasonable request.

Competing Interests

The authors declare that they have no competing interests.

Author details

[1]Key Laboratory of New Processing Technology for Nonferrous Metals and Materials of Ministry of Education, Guilin University of Technology, Guilin 541004, China. [2]Guangxi Key Laboratory of Optical and Electronic Materials and Devices, Guilin University of Technology, Guilin 541004, China. [3]Collaborative Innovation Center for Exploration of Hidden Nonferrous Metal Deposits and Development of New Materials in Guangxi, Guilin University of Technology, Guilin 541004, China.

Received: 21 February 2019 Accepted: 1 August 2019
Published online: 16 August 2019

References

1. Deng L, Shi Z, Peng X, Zhou S (2016) Magnetic calcinated cobalt ferrite/magnesium aluminum hydrotalcite composite for enhanced adsorption of methyl orange. J Alloy Compd 688:101–112
2. Lin C-C, Lin Y-S, Ho J-M (2016) Adsorption of reactive red 2 from aqueous solutions using Fe_3O_4 nanoparticles prepared by co-precipitation in a rotating packed bed. J Alloy Compd 666:153–158

3. Yuan D, Zhou L, Fu D (2017) Adsorption of methyl orange from aqueous solutions by calcined ZnMgAl hydrotalcite. Appl Phys A 123:146
4. Li J, Zhang N, Ng DH (2015) Synthesis of a 3D hierarchical structure of γ-AlO (OH)/Mg-Al-LDH/C and its performance in organic dyes and antibiotics adsorption. J Mater Chem A 3:21106–21115
5. Mecha AC, Onyango MS, Ochieng A, Momba MNB (2017) Evaluation of synergy and bacterial regrowth in photocatalytic ozonation disinfection of municipal wastewater. Sci Total Environ 601-602:626–635
6. Iqbal K, Iqbal A, Kirillov AM, Wang B, Liu W, Tang Y (2017) New Ce-doped MgAl-LDH@Au nanocatalyst for highly efficient reductive degradation of organic contaminants. J Mater Chem A 5:6716–6724
7. Yang Z, Ji S, Gao W, Zhang C, Ren L, Tjiu WW, Zhang Z, Pan J, Liu T (2013) Magnetic nanomaterial derived from graphene oxide/layered double hydroxide hybrid for efficient removal of methyl orange from aqueous solution. J Colloid Interface Sci 408:25–32
8. Yao W, Yu S, Wang J, Zou Y, Lu S, Ai Y, Alharbi NS, Alsaedi A, Hayat T, Wang X (2017) Enhanced removal of methyl orange on calcined glycerol-modified nanocrystallined Mg/Al layered double hydroxides. Chem Eng J 307:476–486
9. Ai L, Zhang C, Meng L (2011) Adsorption of methyl orange from aqueous solution on hydrothermal synthesized Mg-Al layered double hydroxide. J Chem Eng Data 56:4217–4225
10. Tian Z, Li Q, Hou J, Pei L, Li Y, Ai S (2015) Platinum nanocrystals supported on CoAl mixed metal oxide nanosheets derived from layered double hydroxides as catalysts for selective hydrogenation of cinnamaldehyde. J Catal 331:193–202
11. Lafi R, Charradi K, Djebbi MA, Ben Haj Amara A, Hafiane A (2016) Adsorption study of Congo red dye from aqueous solution to Mg-Al-layered double hydroxide. Adv Powder Technol 27:232–237
12. Y. Zheng, N. Li and W. Zhang, Colloids Surf (2012) Preparation of nanostructured microspheres of Zn-Mg-Al layered double hydroxides with high adsorption property, Colloid Surface A 415:195-201
13. Mandal S, Patil VS, Mayadevi S (2012) Alginate and hydrotalcite-like anionic clay composite systems: synthesis, characterization and application studies. Microporous Mesopor Mat 158:241–246
14. Bruna F, Celis R, Real M, Cornejo J (2012) Organo/LDH nanocomposite as an adsorbent of polycyclic aromatic hydrocarbons in water and soil-water systems. J Hazard Mater 225-226:74–80
15. Zhang M, Wu Z, Meng F, Lin H (2019) Facile preparation of grass-like hierarchical structured γ-AlOOH coated stainless steel mesh with superhydrophobic and superoleophilic for highly efficient oil-water separation. Sep Purif Technol 212:347–354
16. X, Zhou, J. Zhang, Y. Ma, H. Tian, Y. Wang, Y. Li, L. Jiang, Q. Cui (2017) The solvothermal synthesis of γ-AlOOH nanoflakes and their compression behaviors under high pressures, RSC Advances 7:4904-4911
17. Wang J, Kang D, Yu X, Ge M, Chen Y (2015) Synthesis and characterization of Mg-Fe-La trimetal composite as an adsorbent for fluoride removal. Chem Eng J 264:506–513
18. Wen T, Wu X, Tan X, Wang X, Xu A (2013) One-pot synthesis of water-swellable Mg-Al layered double hydroxides and graphene oxide nanocomposites for efficient removal of As (V) from aqueous solutions. ACS Appl Mater Interfaces 5:3304–3311
19. Kuśtrowski P, Rafalska-Łasocha A, Majda D, Tomaszewska D, Dziembaj R (2001) Preparation and characterization of new Mg-Al-Fe oxide catalyst precursors for dehydrogenation of ethylbenzene in the presence of carbon dioxide. Solid State Ion 141:237–242
20. Zhang J, Wei S, Lin J, Luo J, Liu S, Song H, Elawad E, Ding X, Gao J, Qi S (2006) Template-free preparation of bunches of aligned boehmite nanowires. J Phys Chem B 110:21680–21683
21. Hajjami M, Ghorbani-Choghamarani A, Ghafouri-Nejad R, Tahmasbi B (2016) Efficient preparation of boehmite silica dopamine sulfamic acid as a novel nanostructured compound and its application as a catalyst in some organic reactions. New J Chem 40:3066–3074
22. Ghorbani-Choghamarani A, Tahmasbi B (2016) The first report on the preparation of boehmite silica sulfuric acid and its applications in some multicomponent organic reactions. New J Chem 40:1205–1212
23. Zou Y, Wang X, Ai Y, Liu Y, Li J, Ji Y, Wang X (2016) Coagulation behavior of graphene oxide on nanocrystallined Mg/Al layered double hydroxides: batch experimental and theoretical calculation study. Environ Sci Technol 50:3658–3667
24. Vitorino NM, Kovalevsky AV, Abrantes JC, Frade J (2015) Hydrothermal synthesis of boehmite in cellular alumina monoliths for catalytic and separation applications. J Eur Ceram Soc 35:3119–3125
25. Yuan X, Wang Y, Wang J, Zhou C, Tang Q, Rao X (2013) Calcined graphene/MgAl-layered double hydroxides for enhanced Cr (VI) removal. Chem Eng J 221:204–213
26. Mohapatra L, Parida K (2016) A review on the recent progress, challenges and perspective of layered double hydroxides as promising photocatalysts. J Mater Chem A 4:10744–10766
27. Murugesan A, Divakaran M, Raveendran P, Nikamanth ABN, Thelly KJ (2019) An eco-friendly porous poly(imide-ether)s for the efficient removal of methylene blue: adsorption kinetics, isotherm, thermodynamics and reuse performances. J Polym Environ 27:1007–1024
28. Cai W, Tan L, Yu J, Jaroniec M, Liu X, Cheng B, Verpoort F (2014) Synthesis of amino-functionalized mesoporous alumina with enhanced affinity towards Cr (VI) and CO_2. Chem Eng J 239:207–215
29. Granados-Correa F, Corral-Capulin N, Olguín M, Acosta-León C (2011) Comparison of the Cd (II) adsorption processes between boehmite (γ-AlOOH) and goethite (α-FeOOH). Chem Eng J 171:1027–1034
30. El Hassani K, Beakou BH, Kalnina D, Oukani E, Anouar A (2017) Effect of morphological properties of layered double hydroxides on adsorption of azo dye methyl orange: a comparative study. Appl Clay Sci 140:124–131
31. Ni Z-M, Xia S-J, Wang L-G, Xing F-F, Pan G-X (2007) Treatment of methyl orange by calcined layered double hydroxides in aqueous solution: adsorption property and kinetic studies. J Colloid Interface Sci 316:284–291
32. Robati D, Mirza B, Rajabi M, Moradi O, Tyagi I, Agarwal S, Gupta V (2016) Removal of hazardous dyes-BR 12 and methyl orange using graphene oxide as an adsorbent from aqueous phase. Chem Eng J 284:687–697
33. Tanhaei B, Ayati A, Lahtinen M, Sillanpää M (2015) Preparation and characterization of a novel chitosan/Al_2O_3/magnetite nanoparticles composite adsorbent for kinetic, thermodynamic and isotherm studies of Methyl Orange adsorption. Chem Eng J 259:1–10
34. Ruan X, Chen Y, Chen H, Qian G, Frost RL (2016) Sorption behavior of methyl orange from aqueous solution on organic matter and reduced graphene oxides modified Ni-Cr layered double hydroxides. Chem Eng J 297:295–303
35. Peng C, Dai J, Yu J, Yin J (2015) Calcined Mg-Fe layered double hydroxide as an absorber for the removal of methyl orange. AIP Adv 5:057138
36. Zhang P, Wang T, Qian G, Wu D, Frost RL (2014) Removal of methyl orange from aqueous solutions through adsorption by calcium aluminate hydrates. J Colloid Interface Sci 426:44–47

Publisher's Note

Springer Nature remains neutral with regard to jurisdictional claims in published maps and institutional affiliations.

Submit your manuscript to a SpringerOpen journal and benefit from:

- ► Convenient online submission
- ► Rigorous peer review
- ► Open access: articles freely available online
- ► High visibility within the field
- ► Retaining the copyright to your article

Submit your next manuscript at ► springeropen.com